# Coronary periarteritis in a patient with multi-organ IgG4-related disease

Yueyang Guo[1], David Ansdell[2], Sharon Brouha[2], Andrew Yen[2*]

*1. School of Medicine, UC San Diego, San Diego, CA, USA*

*2. Department of Radiology, UC San Diego Health System, San Diego, CA, USA*

* **Correspondence:** Andrew Yen, 200 West Arbor Drive, MC8756, San Diego, CA 92103, USA (*acyen@ucsd.edu*)

Radiology Case. 2015 Jan; 9(1):1-17 :: DOI: 10.3941/jrcr.v9i1.1967

ABSTRACT

Immunoglobulin G4-related disease is a recently described systemic clinicopathological entity characterized by immunoglobulin G4-producing plasmacytic infiltration of tissue and frequently by elevated serum immunoglobulin G4 concentration. Manifestations of this disease have been documented in nearly all organs and locations, but coronary artery involvement is not widely recognized. We report the coronary findings of a patient with multi-organ immunoglobulin G4-related disease. Non-electrocardiogram-gated computed tomography of the chest demonstrated nodular and rind-like periarterial soft tissue thickening along the proximal coronary artery segments with improvement following steroid therapy.





# CASE REPORT

## CASE REPORT

An 88-year-old Filipino male was referred in September 2012 for further workup of a left maxillary sinus mass demonstrated on computed tomography (CT) at an outside institution. He presented there with one month's duration of headache, left sinonasal pain and pressure, left facial paresthesia, and left serosanguinous nasal discharge. Physical exam was notable for a fleshy mass filling the left nasal cavity, upward deviation of the left globe, and cranial nerve V2 paresthesia. One month following initial presentation to our institution, his symptoms progressed to include blurry vision, periorbital pruritis, proptosis, malaise, and anorexia with 10-pound weight loss.

Past medical history was significant for hypertension, treated tuberculosis, glaucoma, and benign prostatic hypertrophy. Past surgical history included appendectomy, laser eye surgery for left corneal erosion complicated by nasolacrimal duct obstruction, and cataract surgery. Family history was significant for three sisters with abdominal aortic aneurysms and one sister who died from a cerebral aneurysm. The patient reported remote tobacco use.

*Initial Management*

Clinical findings were suspicious for malignancy. Two successive biopsies of the left maxillary sinus mass at our institution were nondiagnostic, but pathology was notable for significant lymphocytic and plasma cell infiltration with possible spindle cells suggestive of osteosarcoma, plasmacytoma, or carcinoma (Fig. 1).

*Imaging Findings*

The patient subsequently underwent staging CT and positron emission tomography (PET) imaging. CT of the head and neck was notable for a centrally calcified or ossified 5.4 cm x 5.0 cm x 4.6 cm mass within the left maxillary sinus eroding into the ipsilateral infratemporal and pterygopalatine fossae (Fig. 2). The mass showed mild 18F-2-fluoro-2-deoxyglucose (FDG) activity with a maximum standard uptake value (SUV) of 2.4 (Fig. 2). Additionally, CT revealed bilateral symmetrically enlarged and homogeneous lacrimal glands and infraorbital nerves without corresponding FDG-avidity (Figs. 3,4). A non-electrocardiogram (ECG)-gated CT of the chest with contrast was most notable for rind-like periarterial soft tissue thickening and mild nodularity along the proximal coronary artery segments (Figs. 5,6,7). Maximum wall-to-wall coronary arterial diameter measured 1.3 cm, with maximum single wall thickness measuring 0.5 cm. Motion

from the non-ECG-gated acquisition limited evaluation for stenosis. PET scan showed no appreciable FDG activity. Scattered coronary artery calcifications were suggested on the low mA CT attenuation correction sequence of the PET study. The lungs demonstrated a 1.0 cm x 1.0 cm x 1.7 cm left lower lobe irregular nodular opacity with a max SUV of 1.7 (Fig. 8). Abdominal findings included a 1.6 cm x 1.0 cm x 1.4 cm mildly PET-positive perirectal lymph node (max SUV 2.1) and a 4.0 cm x 4.4 cm (in largest trans-axial dimensions) PET-negative infrarenal aortic aneurysm with significant soft plaque (Figs. 9,10).

Differential considerations for the constellation of imaging findings included a left maxillary sinus malignancy with possible lung and nodal metastases, and a lymphoproliferative disorder (such as immunoglobulin G4-related disease or IgG4-RD) in light of initial biopsy findings and soft tissue infiltration involving the lacrimal glands and infraorbital nerves. Vascular findings supported the diagnosis of IgG4-RD but were initially thought to be incidental, with the coronary artery findings possibly due to a vasculitis.

*Further Management*

Based on imaging findings, a left lacrimal gland biopsy was performed in addition to a repeat biopsy of the left maxillary sinus mass. The lacrimal gland displayed significant polytypic plasma cell infiltration without storiform fibrosis or obliterative phlebitis (Fig. 11A). Lymphoid germinal centers were visualized without evidence of malignancy (Fig. 11B). Immunostaining revealed an immunoglobulin G4 to immunoglobulin G (IgG4:IgG) ratio of 0.62 (Fig. 11C). The maxillary sinus mass revealed extensive necrosis with many plasma cells. The sample did not contain clonal populations, cytogenetic abnormalities, or other evidence of malignancy. Serum immunoglobulin levels were notable for elevated IgG at 2025 mg/dL (normal range: 700-1600 mg/dL) and elevated immunoglobulin E (IgE) at 877 IU/mL (normal range: 0-99 IU/mL). The IgG4 level was normal at 28 mg/dL (normal range: 7-89 mg/dL). The patient was started on oral prednisone at 40 mg daily for the diagnosis of IgG4-RD.

*Follow-up*

The patient reported resolution of anorexia and malaise as well as significant improvement in pain and orbital symptoms within two weeks. A gradual steroid taper was started over the next four months without recurrence of symptoms. Six weeks into treatment, IgG and IgE levels decreased to 925 mg/dL and 340 IU/mL, respectively, and further decreased at 11 weeks to 673 mg/dL and 176 IU/mL, respectively. Follow-up CT was performed 7 weeks into therapy and three months after prior imaging. The maxillary sinus mass decreased in size to 3.5 cm x 3.4 cm x 3.3 cm (Fig. 2). The lacrimal glands and infraorbital nerves normalized (Figs. 3,4). A non-ECG-gated CT chest demonstrated a reduction in coronary arterial wall thickness, measuring up to 0.8 cm in wall-to-wall diameter and 0.4 cm in greatest single wall thickness (Figs. 5,6,7). The lung nodule slightly decreased in size to 0.7 cm x 0.9 cm x 1.7 cm (Fig. 8). The perirectal lymph node reduced to 0.9 cm x 0.8 cm x 0.4 cm (Fig. 9). The abdominal aortic aneurysm remained stable in appearance apart from increased non-calcified plaque (Fig. 10).

## DISCUSSION

*Introduction*

IgG4-related disease was first proposed as a new clinicopathological entity by Kamisawa et al. based on immunohistochemical examination of the pancreas and other organs in patients with autoimmune pancreatitis [1]. Since then, conditions long viewed as single organ processes or as part of other systemic diseases (e.g. Mikulicz disease and Küttner tumors) now fall in the spectrum of IgG4-RD [2]. The disease has been described in the pituitary gland, meninges, periorbital tissues, paranasal sinuses, salivary glands, thyroid, lungs, pericardium, breast, arteries, retroperitoneum, pancreas, biliary tree, kidneys, prostate, lymph nodes, and skin [2,3]. As a single or multi-organ disease (with synchronous or metachronous involvement), the condition is characterized by IgG4-positive plasma cell tissue infiltration that may be tumefactive [4,5]. Elevated serum IgG4 is common [6].

*Diagnosis*

Diagnosis of IgG4-RD is currently based on histopathology, although clinical presentation, imaging, and biochemical markers are contributory. As a nascent entity, the diagnosis of IgG4-RD continues to evolve. Currently, according to Deshpande, both a compatible histologic appearance and elevated IgG4-positive plasma cells are requisite for diagnosis [7]. The former includes one or more of a triumvirate of features including: 1) dense lymphoplasmacytic infiltrate with polyclonal plasma cells (and occasional germinal centers), 2) storiform fibrosis, and 3) obliterative phlebitis. A clonal plasma cell population strongly discourages IgG4-RD as a diagnosis. Cutoff points used to determine elevation of IgG4-positive plasma cells depend on site of involvement. Rather than a pure count, one suggested approach is to determine the IgG4:IgG ratio, with a value greater than 0.4 improving specificity. Our patient showed dense polytypic plasma cell infiltration, an IgG4:IgG ratio of 0.62, and corroborative clinical presentation, imaging, and treatment response.

Elevated serum IgG4 levels are neither necessary nor sufficient for diagnosis, as in our case. Elevated serum IgE levels support the diagnosis, particularly if lymph node enlargement is present [8].

*Demographics*

The prevalence of IgG4-RD is difficult to establish due to its relatively recent description in the scientific literature and historically inconsistent terminology. Most of the current case reports originate in Japan, although this is expected to change as awareness of the IgG4-RD entity grows. A study by Umehara et al. estimated the incidence of IgG4-RD in Japan at 0.28-1.08/100,000 population with median age of onset of 58 years [9]. The gender predilection of IgG4-RD depends on the organ system involved [10]. In general, the disease is more common and more severe in males [11,12].

The prevalence of IgG4-related periarteritis has not been studied. This particular manifestation is infrequently reported, and we are aware of only 10 case reports in the literature, nearly all from Japan, that specifically describe IgG4-related

coronary periarteritis [13,14,15,16,17,18,19,20,21,22]. Based on these reports, the mean age of presentation was 71.2 years (range 62-84 years) with 90% being male. Additional case reports likely exist in which a formal diagnosis was not made [23]. Importantly, periarterial abnormalities are difficult to detect with conventional catheter angiography and may be overlooked in the absence of other imaging modalities such as CT and magnetic resonance imaging (MRI) [6].

*Etiology*

The etiology of IgG4-RD is poorly understood. The IgG4 antibody is the least common of the four subclasses of IgG, accounting for 3-6% of total serum IgG. Functionally, it is thought of as an anti-inflammatory immunoglobulin [2,24]. However, IgG4 production appears to depend on T-helper 2 cell cytokines, which are involved in IgE production and allergy [25]. A number of coronary periarteritis cases have noted a prior history of bronchial asthma, and the extant reports suggest an association with allergic rhinitis and asthma [10,13,16,18,26]. Our patient did not have such a history.

The pathologic finding of obliterative phlebitis in this disorder may be due to an allergic reaction against the vasa vasorum, which would explain manifestations of periarteritis [13]. This process may further contribute to chronic inflammation and remodeling, accounting for aneurysm formation and other morphologic changes seen in a number of cases of IgG4-related coronary periarteritis [6].

*Clinical and Imaging Findings*

The spectrum of IgG4-RD in our patient included inflammatory pseudotumor of the maxillary sinus, dacryoadenitis, infraorbital nerve enlargement, periarteritis of the coronary arteries, and lymphadenopathy, with possible pulmonary involvement and aortic periarteritis. In general, the clinical and imaging findings depend on the organ system(s) involved.

IgG4-related coronary periarteritis in our case was striking on non-ECG-gated CT chest, although ECG-gated coronary CT angiography (CTA) would have been complementary or even preferred. IgG4-related coronary periarteritis may manifest as: 1) one or more homogeneous nodular lesions, or pseudotumors, along the coronary artery walls or 2) rinds of soft-tissue attenuation surrounding the coronary arteries. Urabe et al. has described a combination of the two on cardiac CT as "pigs-in-a-blanket" [19]. PET imaging may show increased FDG uptake of coronary periarterial soft tissue [14,19], although this was not evident in our case. Echocardiography was not obtained but may detect large coronary periarterial lesions, evidence of mass effect on nearby structures, and impairment of left ventricular motion and function in the setting of ischemia [13,16,18].

Coronary artery stenosis, ectasia, and aneurysm/pseudoaneurysm formation have been reported in association with IgG4-related coronary periarteritis [13,14,15,16,17,19]. Conventional catheter angiography excels at identifying these sequelae but is limited in its ability to demonstrate associated pseudotumors or wall thickening, particularly in the absence of luminal irregularities. In such circumstances, both intravascular ultrasound (IVUS) and optical coherence tomography (OCT) allow for high-resolution coronary arterial wall imaging via a catheter-based approach and may be useful in the evaluation of IgG4-related coronary periarteritis [27,28]. For example, IVUS identified the extraluminal masses in one case as hypoechoic structures [19], and OCT performed in another revealed circumferential intraluminal calcifications at both aneurysmal and stenotic sites encased by pseudotumors [29]. The less invasive technique of coronary CTA is well suited for the evaluation of both intraluminal and extraluminal abnormalities owing to ECG-gating, which improves temporal resolution and optimizes contrast within the coronary arteries. However, as in our case, routine non-ECG-gated CT chest should allow sufficient visualization of the coronary arteries to support the diagnosis of IG4-related coronary periarteritis.

IgG4-related coronary periarteritis may be associated with symptoms and evidence of coronary ischemia [14,15,19]. Nevertheless, the presence of ischemia does not seem to correlate with degree of vessel wall thickening. For instance, Takei et al. reported an asymptomatic 71-year-old male with IgG4-RD and no evidence of ischemia on stress scintigraphy despite a 2.4 cm x 2.5 cm tumefactive coronary lesion on echocardiography and multiple coronary aneurysms and stenoses on coronary CT angiography [16]. Our patient likewise did not exhibit symptoms of coronary ischemia despite marked coronary involvement.

*Treatment and Prognosis*

IgG4-RD typically responds well to steroid therapy, although relapse may occur [30]. Cases of refractory IgG4-RD have been successfully treated with rituximab and other immunosuppressants [31]. Symptomatic pseudotumors may be managed surgically where accessible, with or without concurrent steroid therapy.

Prior reported cases of coronary periarteritis have followed this pattern of response to steroid therapy with a few exceptions, and to date, there has been no documentation of recurrence in the coronary arteries following treatment. Our case was no different. Pure mass lesions of the coronary arteries without aneurysm or stenosis seem to respond well to oral steroid therapy. When there is evidence of luminal alteration, particularly ectasia, the literature favors surgical resection and coronary artery bypass over steroid therapy due to the potential for steroid-induced vessel wall thinning and, theoretically, rupture [18]. Furthermore, ectatic lesions tended to show minor improvement or continued progression when on steroid therapy, eventually warranting surgical management [14]. In the setting of stenotic lesions, thrombogenicity associated with steroid therapy is also a concern [6]. Given the risk of thrombus formation associated with these vessel abnormalities, antiplatelet agents or anticoagulants may be required [16].

*Differential Diagnosis*

The differential diagnosis for coronary arteritis or periarteritis includes systemic inflammatory diseases causing coronary aneurysms or perivascular masses, and

lymphoproliferative disorders that can encase coronary arteries and mimic perivascular pseudotumor.

Kawasaki disease is an acute febrile childhood vasculitis of medium-sized vessels [32]. Diagnosis is based on distinct clinical criteria including fever, conjunctival injection, mucositis, cervical lymphadenopathy, rash, and peripheral extremity edema or desquamation. Without treatment, Kawasaki disease leads to the formation of coronary aneurysms, including giant aneurysms >0.8 cm in diameter. Continued evolution of the disease leads to fibrosis and stenosis of the involved coronary segments. On CT imaging, there is frequently severe calcification of the coronary arteries [33]. Significant soft-tissue thickening of the vessel walls is not seen.

Polyarteritis nodosa (PAN) is a systemic necrotizing vasculitis of small- to medium-sized arteries and carries an association with viral hepatitis [34]. Multiple organ systems may be involved, although the disease tends to spare the lungs. Coronary involvement may lead to vessel stenosis, dilation, and dissection. In such occurrences, thromboses leading to myocardial infarction and rarely, sudden death, have been reported, although the most common cardiac presentation is heart failure [35,36]. Clinical presentation and overall pattern of organ involvement may serve to differentiate this disorder from IgG4-RD. In terms of coronary imaging, pericoronary pseudotumor is not a well-recognized feature of PAN.

Takayasu arteritis is characterized by an inflammatory infiltration of the media and adventitia of the aorta and its major branches. Epidemiologically, Asian women in their second and third decades of life are at highest risk [37,38]. Common symptoms include fever and fatigue, head and neck pain, upper extremity pain and neuropathy. On CT imaging, arterial stenosis, dilation, and wall thickening may be present [38]. Coronary arterial involvement is rare, with inflammation of the ostia and proximal coronary artery segments leading to ostial and proximal coronary stenoses. Rarer forms of coronary involvement include diffuse or skip lesions throughout the epicardial branches and aneurysm formation. Extensive calcifications may be seen in coronary aneurysms [39].

Churg-Strauss syndrome (eosinophilic granulomatosis with polyangiitis) is a vasculitis of the small vessels with extravascular necrotizing granulomas. The syndrome belongs to a group of vasculitides with elevated anti-neutrophil cytoplasmic antibodies. The mean age of onset is 48 years old [40]. The syndrome evolves through three clinical stages. An initial prodromal stage lasting years consists of allergic rhinitis, nasal polyposis, and bronchial asthma [41]. This is followed by peripheral eosinophilia and transient pulmonary infiltrates. In the final stage, systemic vasculitis occurs, predominantly involving the heart, lungs, skin, peripheral nerves, and kidneys. Cardiac manifestations include myocarditis, heart failure, myocardial infarction, pericarditis, and pericardial effusion [42]. Coronary involvement is rare with few case reports but can include vessel wall abnormalities and giant coronary aneurysms [43,44]. Although bronchial asthma is also associated with IgG4-related periarteritis, the histology and laboratory findings in Churg-Strauss syndrome significantly differ from those of IgG4-RD.

Lymphoma presents with cardiac involvement in 10% of patients [45]. Clinical symptoms include "B symptoms" of fever, weight loss, night sweats, and generalized pruritis. Cardiac-specific presentations depend on site of involvement but frequently include pericardial effusion, heart failure, and atrioventricular (AV) block [46]. Matted mediastinal and pericardiac lymph nodes in lymphoma can surround or encase coronary arteries, mimicking the perivascular thickening of IgG4-related coronary periarteritis on CT imaging. FDG-avidity of lymphoma encasing coronary arteries has been reported [47]. Cardiac ischemia may occur as a result of therapy in lymphoma, although ischemia due to direct compression of the coronary arteries by lymphoma is very rare [48]. A review of systemic findings will assist in the diagnosis, as IgG4-RD predominantly affects extranodal sites. Up to 80% of IgG4-RD patients will have some degree of lymphadenopathy, especially in the mediastinal, abdominal, and axillary regions. In addition, the serum lactate dehydrogenase level is frequently elevated in lymphoma but is usually normal or minimally raised in the setting of IgG4-related lymphadenopathy [49]. In the case of soft tissue masses isolated to the heart, a biopsy is paramount for a definitive diagnosis [46].

Castleman's disease is a rare lymphoproliferative disorder with localized, usually mediastinal, or multicentric presentations and is largely indistinguishable from lymphoma on imaging. Epidemiologically, localized Castleman's disease occurs in young adults whereas multicentric disease occurs in the fifth and sixth decades of life [50]. There is an association with human immunodeficiency virus (HIV) and human herpesvirus-8 (HHV-8) infection. Histology in Castleman's disease is complicated due to a wide variety of subtypes; some patterns resemble the histology of IgG4-RD, and rarely, samples will also have elevated IgG4-positive plasma cells and increased IgG4:IgG ratio. Systemically, serum immunoglobulin A and immunoglobulin M (along with all other antibody types and subtypes) are frequently elevated, unlike IgG4-RD [49]. One case of localized Castleman's disease occurred in the proximal left anterior descending artery. CT imaging revealed a well-defined mass surrounding the artery associated with calcified plaque and 80% stenosis [51]. Pathologic exam of the coronary artery pseudotumor did not reveal a significant predominance of IgG4-positive plasma cells.

Rosai-Dorfman disease is a rare, benign, idiopathic histiocytic and plasmacytic infiltration of lymph nodes. The disease commonly manifests as bilateral painless cervical lymphadenopathy in the first three decades of life in males [52,53]. Cardiac and aortic involvement has been reported [54,55], although the prevalence of cardiac manifestations is less than one percent [56]. By CT imaging, these masses appear as homogeneous soft tissue densities with local enlarged lymph nodes and without significant calcifications. The masses may surround major vessels. Lymph node histology in Rosai-Dorfman disease may also show elevated IgG4-positive plasma cells and IgG4:IgG ratio [7].

## TEACHING POINT

IgG4-related coronary periarteritis can be detected on ECG- or non-ECG-gated chest CT and should be considered in the differential diagnosis for nodular or rind-like coronary arterial wall thickening. Stenosis, luminal ectasia, and aneurysm formation may be associated, and metabolic activity on PET imaging is variable.

## REFERENCES

1. Kamisawa T, Funata N, Hayashi Y, et al. A new clinicopathological entity of IgG4-related autoimmune disease. J Gastroenterol. 2003;38(10):982-4. PMID: 14614606

2. Guma M, Firestein GS. IgG4-related diseases. Best Pract Res Clin Rheumatol. 2012 Aug;26(4):425-38. PMID: 23040358

3. Wong S, Lam WY, Wong WK, Lee KC. Hypophysitis presented as inflammatory pseudotumor in immunoglobulin G4-related systemic disease. Hum Pathol. 2007 Nov;38(11):1720-3. PMID: 17954209

4. Okazaki K, Uchida K, Koyabu M, Miyoshi H, Takaoka M. Recent advances in the concept and diagnosis of autoimmune pancreatitis and IgG4-related disease. J Gastroenterol. 2011 Mar;46(3):277-88. PMID: 21452084

5. Sah RP, Chiari ST, Pannala R, et al. Differences in clinical profile and relapse rate of type 1 versus type 2 autoimmune pancreatitis. Gastroenterology. 2010 Jul;139(1):140-8. PMID: 20353791

6. Ishizaka N. IgG4-related disease underlying the pathogenesis of coronary artery disease. Clin Chim Acta. 2013 Jan;415:220-5. PMID: 23146869

7. Deshpande V. The pathology of IgG4-related disease: critical issues and challenges. Semin Diagn Pathol. 2012 Nov;29(4):191-6. PMID: 23068297

8. Stone JH. IgG4-related disease: nomenclature, clinical features, and treatment. Semin Diagn Pathol. 2012 Nov;29(4):177-90. PMID: 23068296

9. Umehara H, Okazaki K, Masaki Y, et al. A novel clinical entity, IgG4-related disease (IgG4RD): general concepts and details. Mod Rheumatol. 2012 Feb;22(1):1-14. PMID: 21881964

10. Zen Y, Nakanuma Y. IgG4-related disease: a cross-sectional study of 114 cases. Am J Surg Pathol. 2010 Dec;34(12):1812-9. PMID: 21107087

11. Andrew N, Kearney D, Selva D. IgG4-related orbital disease: a meta-analysis and review. Acta Ophthalmol. 2012 Sep 11. [Epub ahead of print]. PMID: 22963447

12. Khosroshahi A, Stone JH. A clinical overview of IgG4-related systemic disease. Curr Opin Rheumatol. 2011 Jan;23(1):57-66. PMID: 21124086

13. Matsumoto Y, Kasashima S, Kawashima A, et al. A case of multiple immunoglobulin G4-related periarteritis: a tumorous lesion of the coronary artery and abdominal aortic aneurysm. Hum Pathol. 2008 Jun;39(6):975-80. PMID: 18430457

14. Ikutomi M, Matsumura T, Iwata H, et al. Giant tumororous lesions surrounding the right coronary artery associated with immunoglobulin-G4-related systemic disease. Cardiology. 2011;120(1):22-6. PMID: 22094884

15. Tanigawa J, Daimon M, Murai M, Katsumata T, Tsuji M, Ishizaka N. Immunoglobulin G4-related coronary periarteritis in a patient presenting with myocardial ischemia. Hum Pathol. 2012 Jul;43(7):1131-4. PMID: 22401772

16. Takei H, Nagasawa H, Sakai R, et al. A case of multiple giant coronary aneurysms and abdominal aortic aneurysm coexisting with IgG4-related disease. Intern Med. 2012;51(8):963-7. PMID: 22504260

17. Debonnaire P, Bammens B, Blockmans D, Herregods MC, Dubois C, Voigt JU. Multimodality imaging of giant coronary aneurysms in immunoglobulin g4-related sclerosing disease. J Am Coll Cardiol. 2012 Apr;59(14):e27. PMID: 22464268

18. Kusumoto S, Kawano H, Takeno M, et al. Mass lesions surrounding coronary artery associated with immunoglobulin G4-related disease. J Cardiol Cases [serial online]. 2012; vol 5, no. 3. Available at: http://www.journalofcardiologycases.com/article/S1878-5409%2812%2900012-6/fulltext. Accessed March 5, 2013.

19. Urabe Y, Fujii T, Kurushima S, Tsujiyama S, Kihara Y. Pigs-in-a-blanket coronary arteries: a case of immunoglobulin G4-related coronary periarteritis assessed by computed tomography coronary angiography, intravascular ultrasound, and positron emission tomography. Circ Cardiovasc Imaging. 2012 Sep 1;5(5):685-7. PMID: 22991288

20. Fujii T, Tsushima H, Masada K, et al. A case report of acute myocardial infarction associated with coronary artery aneurysm and IgG-related periarteritis. Nihon Nouson Igakkai Gakujyutu Soukai Syourokusyu. 2010;59:108. [in Japanese]

21. Okamoto M, Nagumo M, Goto T, Yoshitake A, Miki T, Osumi K. A case of immunoglobulin G4-related cardiac tumor around the coronary artery. Jpn J Cardiovasc Surg. 2010 May;39(4):230-233

22. Ichihara Y, Tsuchiya K, Nakajima M, Kaku Y, Koyama T. A case report of surgical repair for IgG4-related coronary artery aneurysm. The 155th meeting of The Kanto

Koushinetsu area in The Japanese Association for Thoracic Surgery Abstract. 2011; p. 21. [in Japanese].

23. Maturen KE, Sundaram B, Marder W, Swartz RD. Coronary artery involvement in idiopathic retroperitoneal fibrosis: computed tomographic findings. J Thorac Imaging. 2012 Mar;27(2):W35-7. PMID: 21516043

24. Aalberse RC, Stapel SO, Schuurman J, Rispens T. Immunoglobulin G4: an odd antibody. Clin Exp Allergy. 2009 Apr;39(4):469-77. PMID: 19222496

25. Nirula A, laser SM, Kaled SL, Taylor FR. What is IgG4? A review of the biology of a unique immunoglobulin subtype. Curr Opin Rheumatol. 2011 Jan;23(1):119-24. PMID: 21124094

26. Masaki Y, Dong L, Kurose N, et al. Proposal for a new clinical entity, IgG4-positive multiorgan lymphoproliferative syndrome: analysis of 64 cases of IgG4-related disorders. Ann Rheum Dis. 2009 Aug;68(8):1310-5. PMID: 18701557

27. Prati F, Regar E, Mintz GS, et al. Expert review document on methodology, terminology, and clinical applications of optical coherence tomography: physical principles, methodology of image acquisition, and clinical application for assessment of coronary arteries and atherosclerosis. Eur Heart J. 2010 Feb;31(4):401-15. PMID: 19892716

28. Jang IK, Bouma BE, Kang DH, et al. Visualization of coronary atherosclerotic plaques in patients using optical coherence tomography: comparison with intravascular ultrasound. J Am Coll Cardiol. 2002 Feb;39(4):604-9. PMID: 11849858

29. Tanigawa J, Ishizaka N. Optical coherence tomography in IgG4-related coronary periarteritis. Intern Med. 2013;52(2):289. PMID: 23318866

30. Horger M, Lamprecht HG, Bares R, et al. Systemic IgG4-related sclerosing disease: spectrum of imaging findings and differential diagnosis. AJR Am J Roentgenol. 2012 Sep;199(3):W276-82. PMID: 22915418

31. Lindau RH, Su YB, Kobayashi R, Smith RB. Immunoglobulin G4-related sclerosing disease of the paranasal sinus. Head Neck. 2013 Oct;35(10):E321-4. PMID: 23047661

32. Mavrogeni S, Papadopoulos G, Karanasios E, Cokkinos DV. How to image Kawasaki disease: a validation of different imaging techniques. Int J Cardiol. 2008 Feb;124(1):27-31. PMID: 17434612

33. Akagi T. Interventions in Kawasaki disease. Pediatr Cardiol. 2005 Mar-Apr;26(2):206-12. PMID: 15868317

34. Guillevin L. Infections in vasculitis. Best Pract Res Clin Rheumatol. 2013 Feb;27(1):19-31. PMID: 23507054

35. Canpolar C, Dural M, Atalar E. Acute inferior myocardial infarction in a young female patient with polyarteritis nodosa. Herz. 2012 Jun;37(4):461-3. PMID: 22301728

36. Shields LB, Burge M, Hunsaker JC 3rd. Sudden death due to polyarteritis nodosa. Forensic Sci Med Pathol. 2012 Sep;8(3):290-5. PMID: 21983834

37. Rav-Acha M, Plot L, Peled N, Amital H. Coronary involvement in Takayasu's arteritis. Autoimmun Rev. 2007 Sep;6(8):566-71. PMID: 17854750

38. Isobe M. Takayasu arteritis revisited: current diagnosis and treatment. Int J Cardiol. 2013 Sep 20;168(1):3-10. PMID: 23415176

39. Seyahi E, Ucgul A, Olgun DC, et al. Aortic and coronary calcifications in Takayasu arteritis. Semin Arthritis Rheum. 2013 Aug;43(1):96-104. PMID: 23351614

40. Pagnoux C, Guilpain P, Guillevin L. Churg-Strauss syndrome. Curr Opin Rheumatol. 2007 Jan;19(1):25-32. PMID: 17143092

41. Yevich I. Necrotizing vasculitis with granulomatosis. Int J Dermatol. 1988 Oct;27(8):540-6. PMID: 3061945

42. Dennert RM, van Paassen P, Schalla S, et al. Cardiac involvement in Churg-Strauss syndrome. Arthritis Rheum. 2010 Feb;62(2):627-34. PMID: 20112390

43. Hellemans S, Dens J, Knockaert D. Coronary involvement in the Churg-Strauss syndrome. Heart. 1997 Jun;77(6):576-8. PMID: 9227307

44. Htun P, Horger M, Gawaz M, Fateh-Moghadam S. Clinical images: giant coronary artery aneurysms and eosinophilic granulomatosis with polyangiitis. Arthritis Rheum. 2013 May;65(5):1406.

45. McDonnell PJ, Mann RB, Bulkley BH. Involvement of the heart by malignant lymphoma: a clinicopathologic study. Cancer. 1982 Mar;49(5):944-51. PMID: 7037154

46. Miguel CE, Bestetti RB. Primary cardiac lymphoma. Int J Cardiol. 2011 Jun;149(3):358-63. PMID: 20227122

47. Kikuchi Y, Oyama-Manabe N, Manabe O, et al. Imaging characteristics of cardiac dominant diffuse large B-cell lymphoma demonstrated with MDCT and PET/CT. Eur J Nucl Med Mol Imaging. 2013 Sep;40(9):1337-44. PMID: 23653245

48. Nagasako Y, Akaeda S, Yanase F, et al. Ischemic heart disease due to compression of the coronary arteries by malignant lymphoma. Intern Med. 2012;51(20):2949-52. PMID: 23064574

49. Cheuk W, Chan JK. Lymphadenopathy of IgG4-related disease: an underdiagnosed and overdiagnosed entity. Semin Diagn Pathol. 2012 Nov;29(4):226-34. PMID: 23068302

50. Herrada J, Cabanillas F, Rice L, Manning J, Pugh W. The clinical behavior of localized and multicentric Castleman disease. Ann Intern Med. 1998 Apr;128(8):657-62. PMID: 9537940

51. Just PA, Cazes A, Goebel H, Mousseaux E, Fabiani JN, Bruneval P. A case of pericoronary pseudotumor due to localized Castleman's disease. Cardiovasc Pathol. 2009 Nov-Dec;18(6):375-8. PMID: 18436453

52. La Barge DV 3rd, Salzman KL, Harnsberger HR, et al. Sinus histiocytosis with massive lymphadenopathy (Rosai-Dorfman disease): imaging manifestations in the head and neck. AJR Am J Roentgenol. 2008 Dec;191(6):W299-306. PMID: 19020219

53. Molina-Garrido MJ, Guillén-Ponce C. Extranodal rosai-dorfman disease with cutaneous and periodontal involvement: a rare presentation. Case Rep Oncol. 2011 Feb;4(1):96-100. PMID: 21475597

54. Yontz L, Franco A, Sharma S, Lewis K, McDonough C. A case of Rosai-Dorfman disease in a pediatric patient with cardiac involvement. J Radiol Case Rep. 2012 Jan;6(1):1-8. PMID: 22690274

55. Sarraj A, Zarra KV, Jimenez Borreguero LJ, Caballero P, Nuche JM. Isolated cardiac involvement of Rosai-Dorfman disease. Ann Thorac Surg. 2012 Dec;94(6):2118-20. PMID: 23176929

56. Gaitonde S. Multifocal, extranodal sinus histiocytosis with massive lymphadenopathy: an overview. Arch Pathol Lab Med. 2007 Jul;131(7):1117-21. PMID: 17617001

## FIGURES

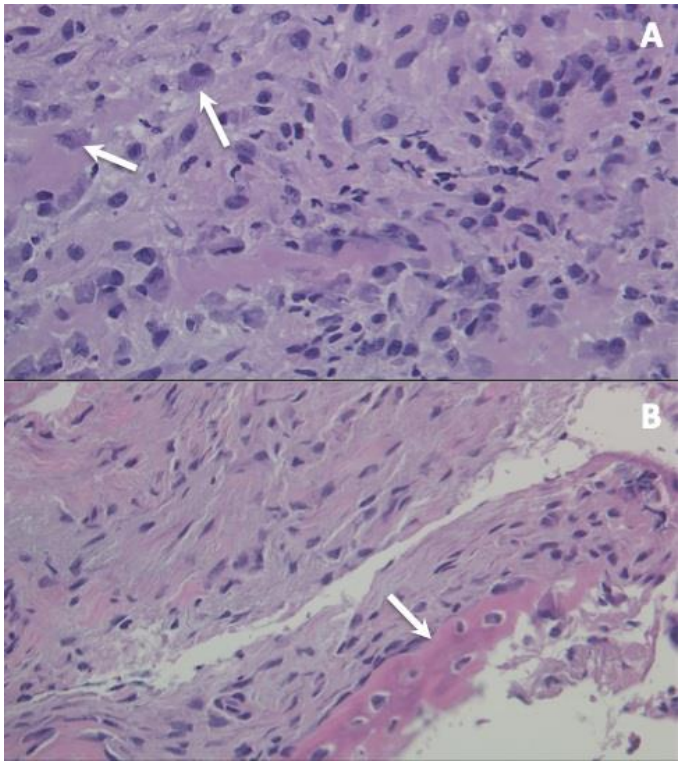


**Figure 1:** 88-year-old male with IgG4-related disease. FINDINGS: First biopsy of the left maxillary sinus mass (H&E stain, magnification 600x). A. Plasma cells (arrows) intermixed with other lymphocytes. B. Osteoid (arrow) alongside spindle cells.

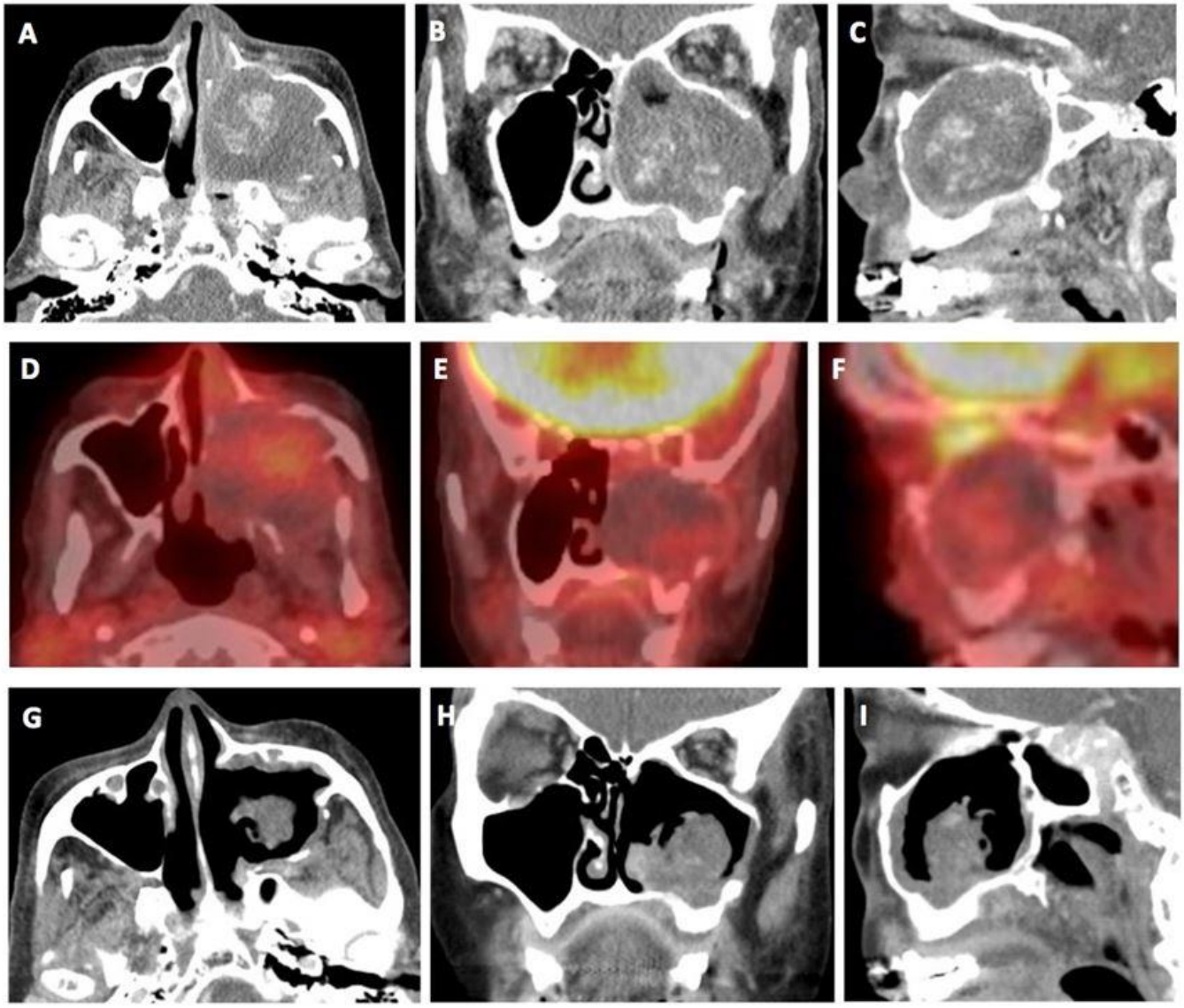






**Figure 2:** 88-year-old male with IgG4-related disease.

FINDINGS: Images are axial, coronal, and sagittal from left to right. A-C. A contrast-enhanced CT scan of the head and neck in the venous phase demonstrates a centrally calcified or ossified 5.4 cm x 5.0 cm x 4.6 cm mass within the left maxillary sinus eroding into the ipsilateral infratemporal fossa. D-F. A concurrent fused PET-CT demonstrates mild FDG activity (max SUV 2.4). G-I. Three months later, and 7 weeks into steroid treatment, a follow-up contrast-enhanced CT scan of the face in the venous phase demonstrates decreased size of the mass measuring 3.5 cm x 3.4 cm x 3.3 cm.

TECHNIQUE: A-C. 64-slice CT, 100-180 mA, 120 kVp, 100 mL Omnipaque 350 IV contrast at 2.5 mL/sec, standard algorithm, 2.5 mm slice thickness. D-F. PET-CT, 18.6 mCi F18-FDG, 1 hour uptake period, multi-bed 3D acquisition, low mA CT attenuation correction (mA 30-65, kVp 140), axial 3.27 mm, coronal 5.47 mm, and sagittal 5.47 mm slice thickness. G-I. 64-slice CT, 150-500 mA, 120 kVp, 100 mL Omnipaque 350 IV contrast at 2.5 mL/sec, standard algorithm, axial 2.5 mm, coronal 5 mm, and sagittal 5 mm slice thickness.

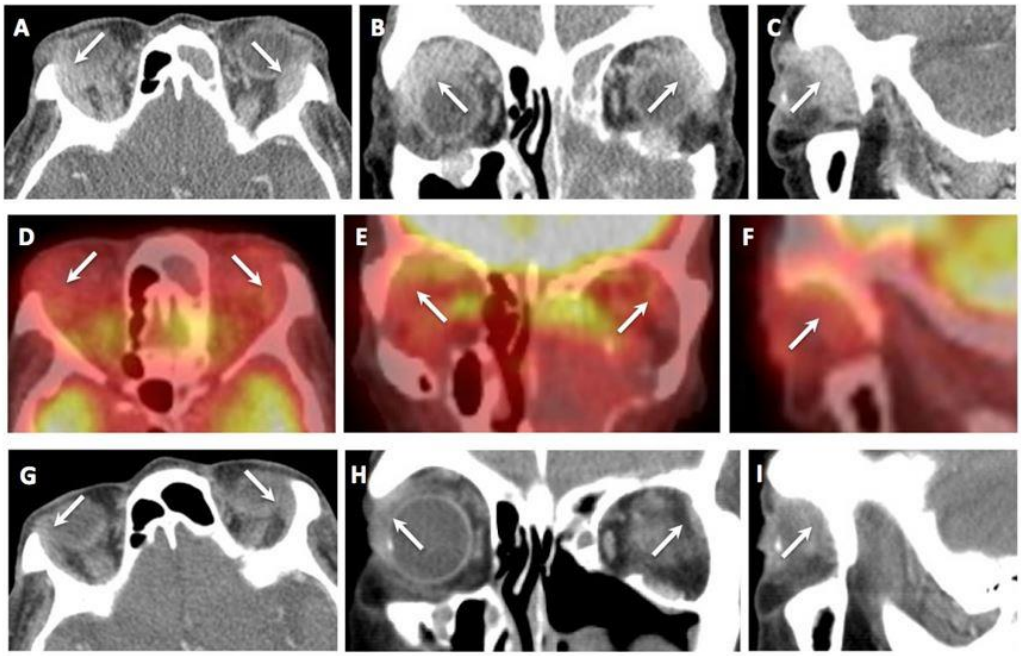


**Figure 3:** 88-year-old male with IgG4-related disease. FINDINGS: Images are axial, coronal, and sagittal from left to right. A-C. A contrast-enhanced CT scan of the head and neck in the venous phase demonstrates bilateral symmetrically enlarged and homogeneous lacrimal glands (arrows). D-F. A concurrent fused PET-CT demonstrates no FDG avidity (arrows). G-I. Three months later, and 7 weeks into steroid treatment, a follow-up contrast-enhanced CT scan of the face in the venous phase demonstrates normalization (arrows). TECHNIQUE: A-C. 64-slice CT, 100-180 mA, 120 kVp, 100 mL Omnipaque 350 IV contrast at 2.5 mL/sec, standard algorithm, 2.5 mm slice thickness. D-F. PET-CT, 18.6 mCi F18-FDG, 1 hour uptake period, multi-bed 3D acquisition, low mA CT attenuation correction (mA 30-65, kVp 140), axial 3.27 mm, coronal 5.47 mm, and sagittal 5.47 mm slice thickness. G-I. 64-slice CT, 150-500 mA, 120 kVp, 100 mL Omnipaque 350 IV contrast at 2.5 mL/sec, standard algorithm, axial 2.5 mm, coronal 5 mm, and sagittal 5 mm slice thickness.





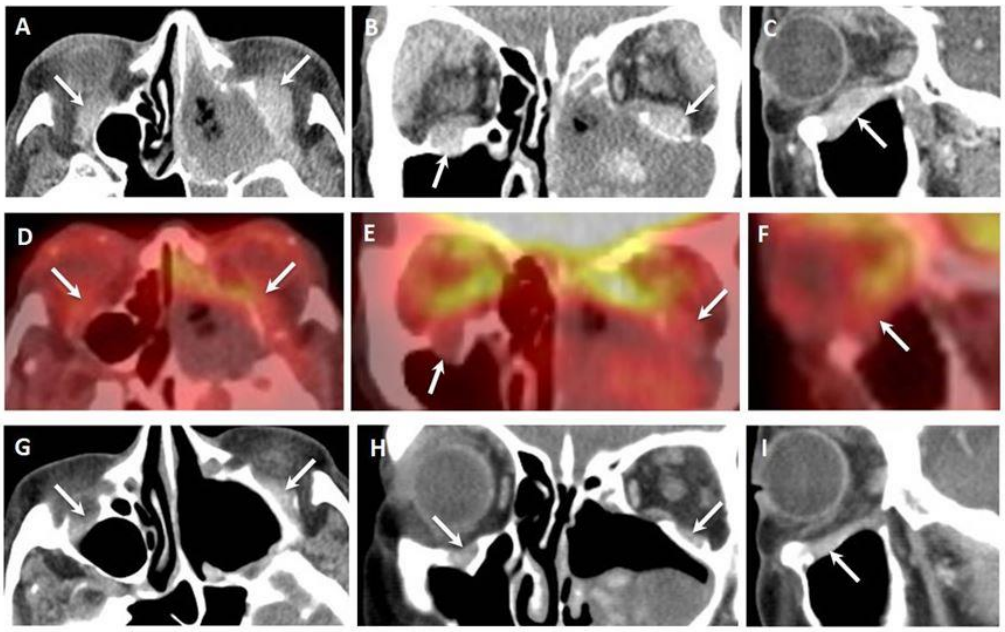


**Figure 4:** 88-year-old male with IgG4-related disease. FINDINGS: Images are axial, coronal, and sagittal from left to right. A-C. A contrast-enhanced CT scan of the head and neck in the venous phase demonstrates bilateral symmetrically enlarged and homogeneous infraorbital nerves (arrows). D-F. A concurrent fused PET-CT demonstrates no FDG avidity (arrows). G-I. Three months later, and 7 weeks into steroid treatment, a follow-up contrast-enhanced CT scan of the face in the venous phase demonstrates normalization (arrows). TECHNIQUE: A-C. 64-slice CT, 100-180 mA, 120 kVp, 100 mL Omnipaque 350 IV contrast at 2.5 mL/sec, standard algorithm, 2.5 mm slice thickness. D-F. PET-CT, 18.6 mCi F18-FDG, 1 hour uptake period, multi-bed 3D acquisition, low mA CT attenuation correction (mA 30-65, kVp 140), axial 3.27 mm, coronal 5.47 mm, and sagittal 5.47 mm slice thickness. G-I. 64-slice CT, 150-500 mA, 120 kVp, 100 mL Omnipaque 350 IV contrast at 2.5 mL/sec, standard algorithm, axial 2.5 mm, coronal 5 mm, and sagittal 5 mm slice thickness.

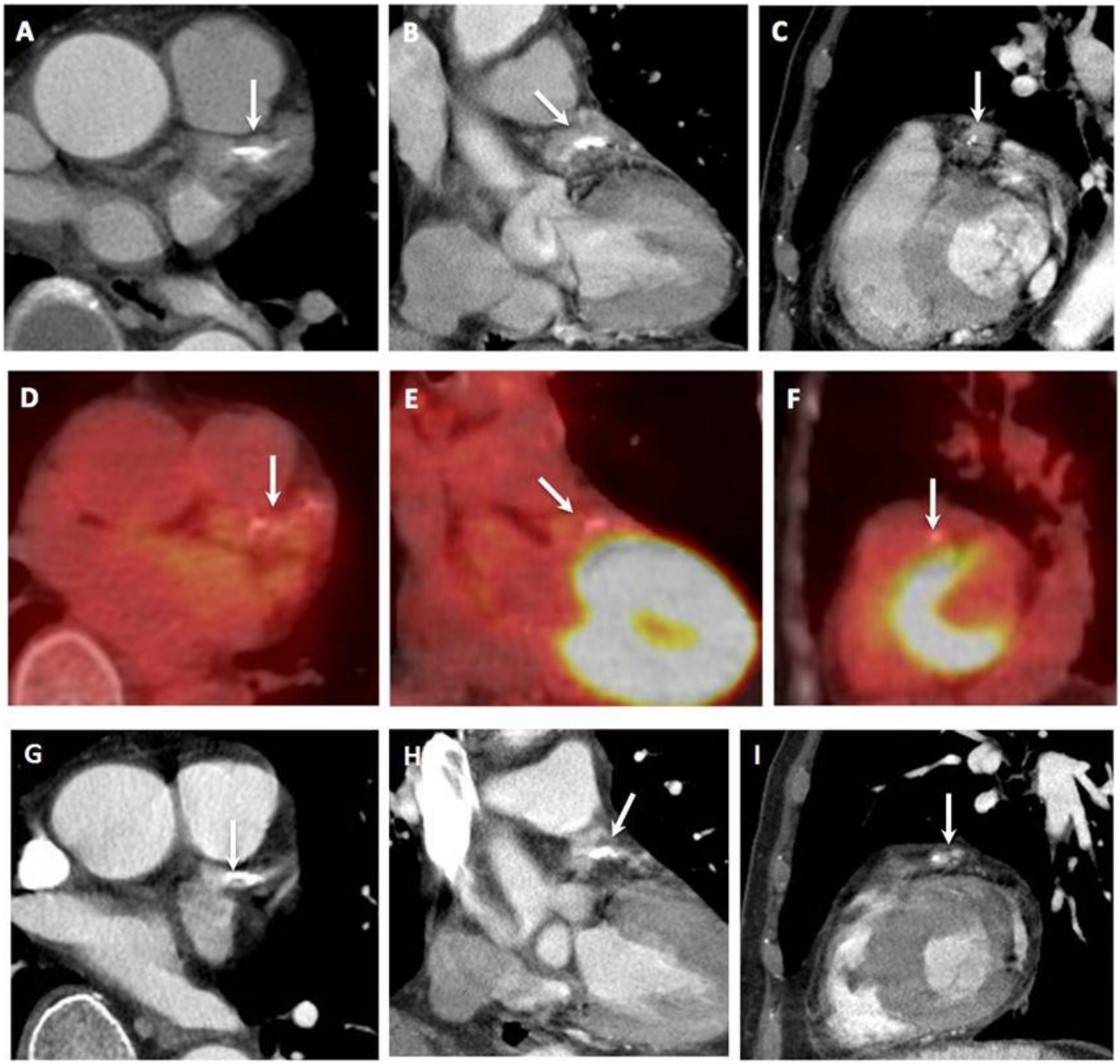






**Figure 5:** 88-year-old male with IgG4-related disease.

FINDINGS: Images are axial, coronal, and sagittal from left to right. A-C. A non-ECG-gated contrast-enhanced CT scan of the chest in the late arterial phase demonstrates rind-like periarterial soft tissue thickening (max 1.2 cm wall-to-wall, max 0.5 cm single wall) along the proximal left anterior descending coronary artery (arrows). D-F. A concurrent fused PET-CT shows no appreciable FDG activity (arrows). G-I. Three months later, and 7 weeks into steroid treatment, a follow-up non-ECG-gated contrast-enhanced CT scan of the chest in the late arterial phase demonstrates a reduction in wall thickness (max 0.5 cm wall-to-wall, max 0.2 cm single wall) (arrows).

TECHNIQUE: A-C. 64-slice CT, 300-600 mA, 100 kVp, 100 mL Omnipaque 350 IV contrast at 2.5 mL/sec, 2.6 sec scan time, standard algorithm, 2.5 mm slice thickness. D-F. PET-CT, 18.6 mCi F18-FDG, 1 hour uptake period, multi-bed 3D acquisition, low mA CT attenuation correction (mA 30-65, kVp 140), axial 3.27 mm, coronal 5.47 mm, and sagittal 5.47 mm slice thickness. G-I. 64-slice CT, 200-600 mA, 100 kVp, 100 mL Omnipaque 350 IV contrast at 2.5 mL/sec, 2.6 sec scan time, standard algorithm, axial 2.5 mm, coronal 2 mm, and sagittal 2 mm slice thickness.

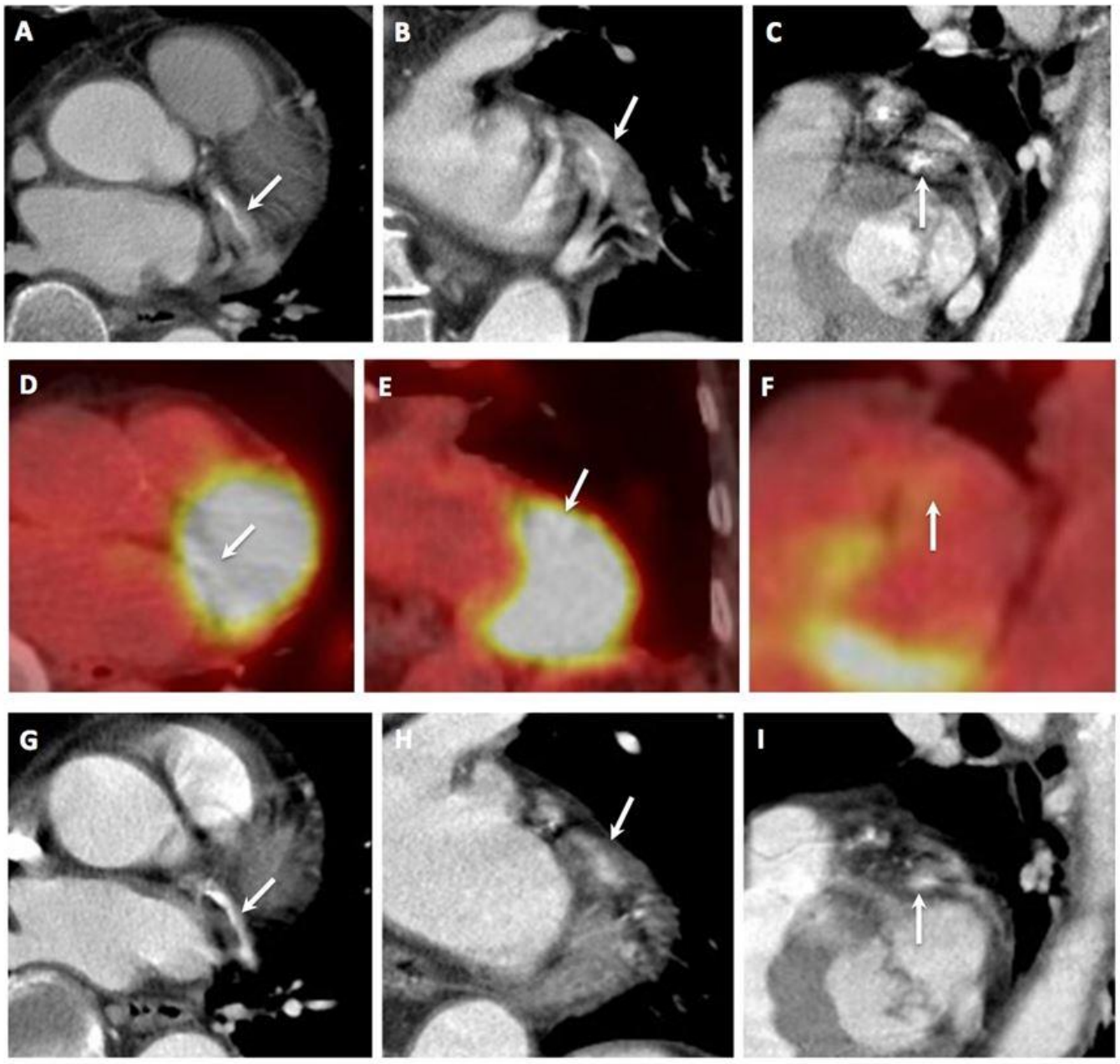






**Figure 6:** 88-year-old male with IgG4-related disease.

FINDINGS: Images are axial, coronal, and sagittal from left to right. A-C. A non-ECG-gated contrast-enhanced CT scan of the chest in the late arterial phase demonstrates rind-like periarterial soft tissue thickening (max 1.0 cm wall-to-wall, max 0.4 cm single wall) along the proximal left circumflex coronary artery (arrows). D-F. A concurrent fused PET-CT shows no appreciable FDG activity (arrows). G-I. Three months later, and 7 weeks into steroid treatment, a follow-up non-ECG-gated contrast-enhanced CT scan of the chest in the late arterial phase demonstrates a slight reduction in wall thickness (max 0.8 cm wall-to-wall, max 0.4 cm single wall) (arrows).

TECHNIQUE: A-C. 64-slice CT, 300-600 mA, 100 kVp, 100 mL Omnipaque 350 IV contrast at 2.5 mL/sec, 2.6 sec scan time, standard algorithm, 2.5 mm slice thickness. D-F. PET-CT, 18.6 mCi F18-FDG, 1 hour uptake period, multi-bed 3D acquisition, low mA CT attenuation correction (mA 30-65, kVp 140), axial 3.27 mm, coronal 5.47 mm, and sagittal 5.47 mm slice thickness. G-I. 64-slice CT, 200-600 mA, 100 kVp, 100 mL Omnipaque 350 IV contrast at 2.5 mL/sec, 2.6 sec scan time, standard algorithm, axial 2.5 mm, coronal 2 mm, and sagittal 2 mm slice thickness.

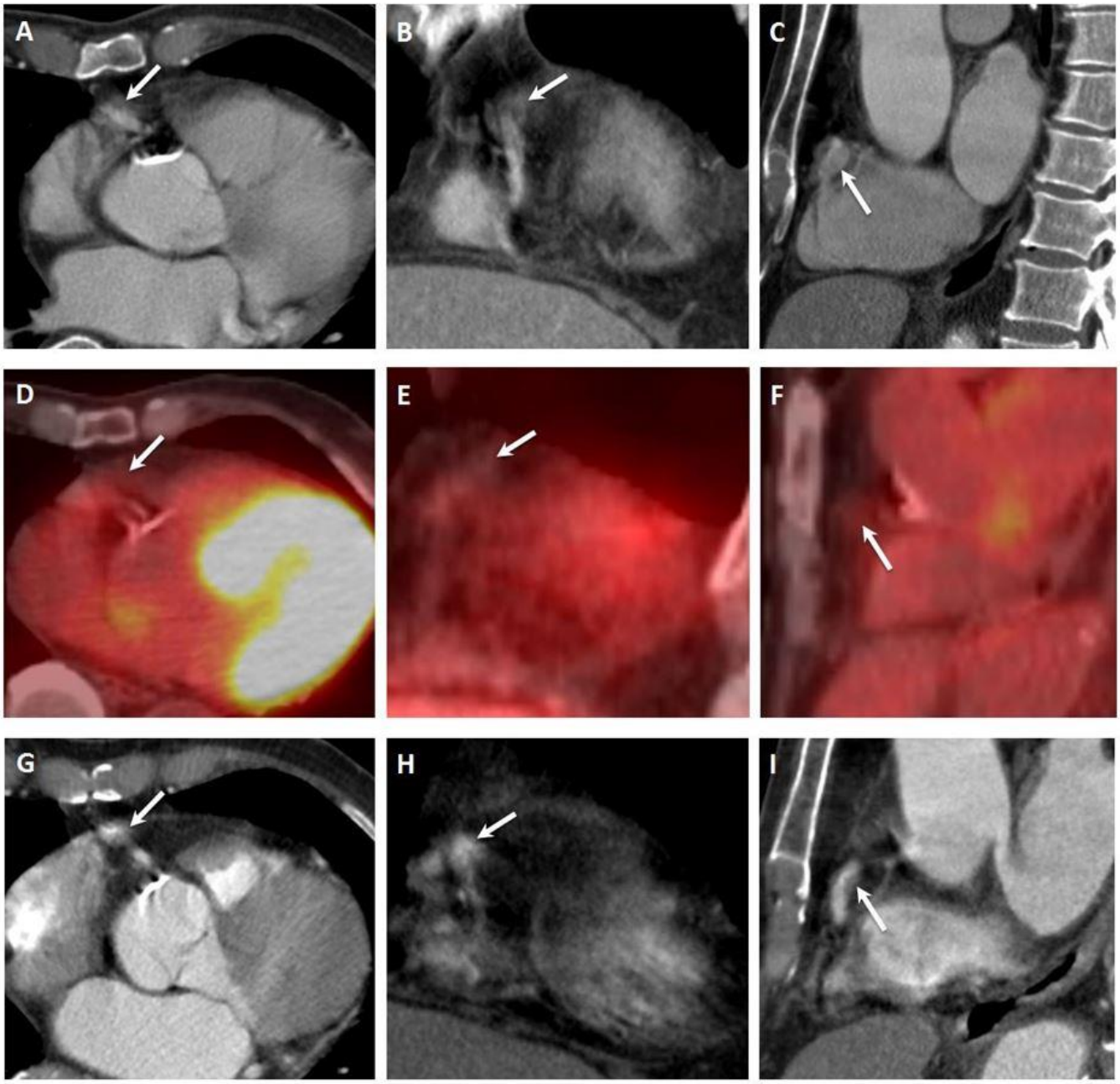






**Figure 7:** 88-year-old male with IgG4-related disease.

FINDINGS: Images are axial, coronal, and sagittal from left to right. A-C. A non-ECG-gated contrast-enhanced CT scan of the chest in the late arterial phase demonstrates nodular and rind-like periarterial soft tissue thickening (max 1.3 cm wall-to-wall, max 0.5 cm single wall) along the proximal right coronary artery (arrows). D-F. A concurrent fused PET-CT shows no appreciable FDG activity (arrows). G-I. Three months later, and 7 weeks into steroid treatment, a follow-up non-ECG-gated contrast-enhanced CT scan of the chest in the late arterial phase demonstrate a slight reduction in wall thickness (max 0.8 cm wall-to-wall, max 0.3 cm single wall) (arrows).

TECHNIQUE: A-C. 64-slice CT, 300-600 mA, 100 kVp, 100 mL Omnipaque 350 IV contrast at 2.5 mL/sec, 2.6 sec scan time, standard algorithm, 2.5 mm slice thickness. D-F. PET-CT, 18.6 mCi F18-FDG, 1 hour uptake period, multi-bed 3D acquisition, low mA CT attenuation correction (mA 30-65, kVp 140), axial 3.27 mm, coronal 5.47 mm, and sagittal 5.47 mm slice thickness. G-I. 64-slice CT, 200-600 mA, 100 kVp, 100 mL Omnipaque 350 IV contrast at 2.5 mL/sec, 2.6 sec scan time, standard algorithm, axial 2.5 mm, coronal 2 mm, and sagittal 2 mm slice thickness.

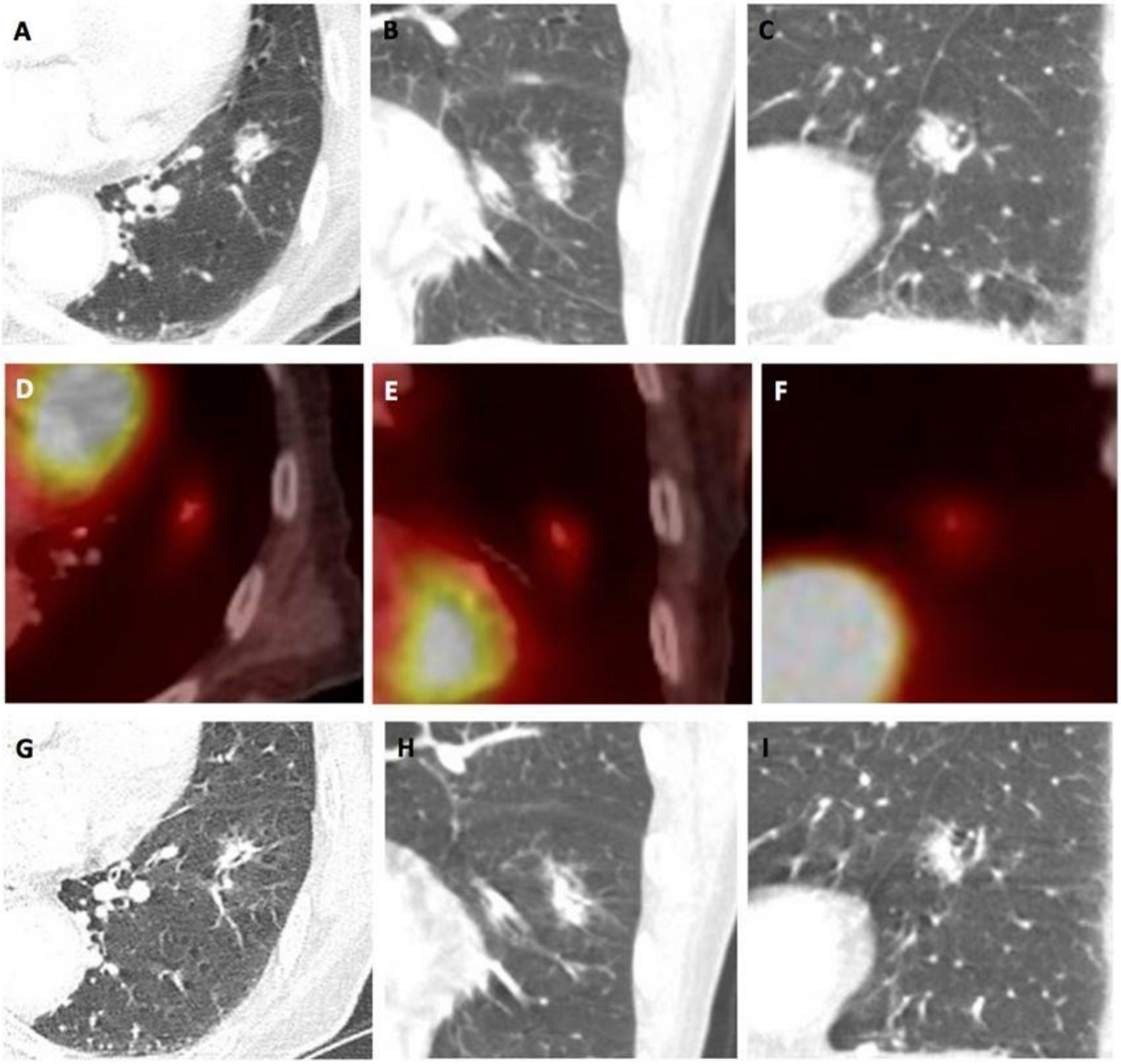






**Figure 8:** 88-year-old male with IgG4-related disease.

FINDINGS: Images are axial, coronal, and sagittal from left to right. A-C. A contrast-enhanced CT scan of the chest in the late arterial phase demonstrates a 1.0 cm x 1.0 cm x 1.7 cm irregular nodular lung opacity in the left lower lobe. D-F. A concurrent fused PET-CT shows mild FDG avidity with a max SUV of 1.7. G-I. Three months later, and 7 weeks into steroid treatment, a follow-up contrast-enhanced CT scan of the chest in the late arterial phase demonstrates a slight decrease in size measuring 0.7 cm x 0.9 cm x 1.7 cm.

TECHNIQUE: A-C. 64-slice CT, 300-600 mA, 100 kVp, 100 mL Omnipaque 350 IV contrast at 2.5 mL/sec, bone algorithm (axial) at 1.25 mm slice thickness, standard algorithm (coronal, sagittal) at 2.5 mm slice thickness. D-F. PET-CT, 18.6 mCi F18-FDG, 1 hour uptake period, multi-bed 3D acquisition, low mA CT attenuation correction (mA 30-65, kVp 140), axial 3.27 mm, coronal 5.47 mm, and sagittal 5.47 mm slice thickness. G-I. 64-slice CT, 200-600 mA, 100 kVp, 100 mL Omnipaque 350 IV contrast at 2.5 mL/sec, bone plus algorithm (axial) at 1.25 mm slice thickness, standard algorithm (coronal, sagittal) at 2 mm slice thickness.

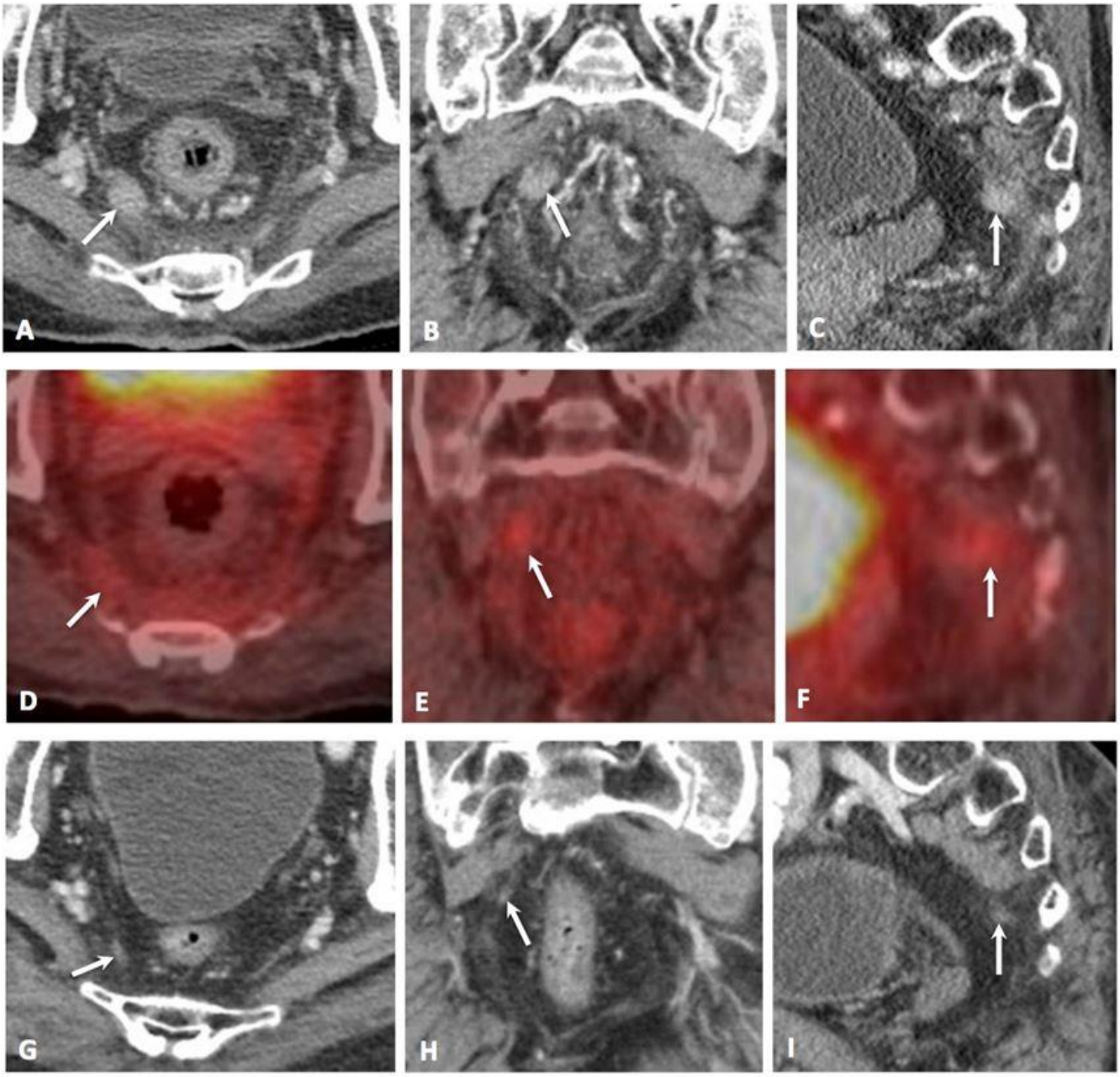


**Figure 9:** 88-year-old male with IgG4-related disease.

FINDINGS: Images are axial, coronal, and sagittal from left to right. A-C. A contrast-enhanced CT scan of the pelvis in the portal venous phase demonstrates a 1.6 cm x 1.0 cm x 1.4 cm right perirectal lymph node (arrows). D-F. A concurrent fused PET-CT shows mild FDG avidity (max SUV 2.1). G-I. Three months later, and 7 weeks into steroid treatment, a follow-up contrast-enhanced CT scan of the pelvis in the portal venous phase demonstrates a slight decrease in size measuring 0.9 cm x 0.8 cm x 0.4 cm (arrows).

TECHNIQUE: A-C. 64-slice CT, 200-230 mA, 120 kVp, 100 mL Omnipaque 350 IV contrast at 2.5 mL/sec, standard algorithm, axial 3.75 mm, coronal 2.5 mm, and sagittal 2.5 mm slice thickness. D-F. PET-CT, 18.6 mCi F18-FDG, 1 hour uptake period, multi-bed 3D acquisition, low mA CT attenuation correction (mA 30-65, kVp 140), axial 3.27 mm, coronal 5.47 mm, and sagittal 5.47 mm slice thickness. G-I. 64-slice CT, 210-250 mA, 120 kVp, 100 mL Omnipaque 350 IV contrast at 2.5 mL/sec, standard algorithm, axial 3.75 mm, coronal 3 mm, and sagittal 3 mm slice thickness.

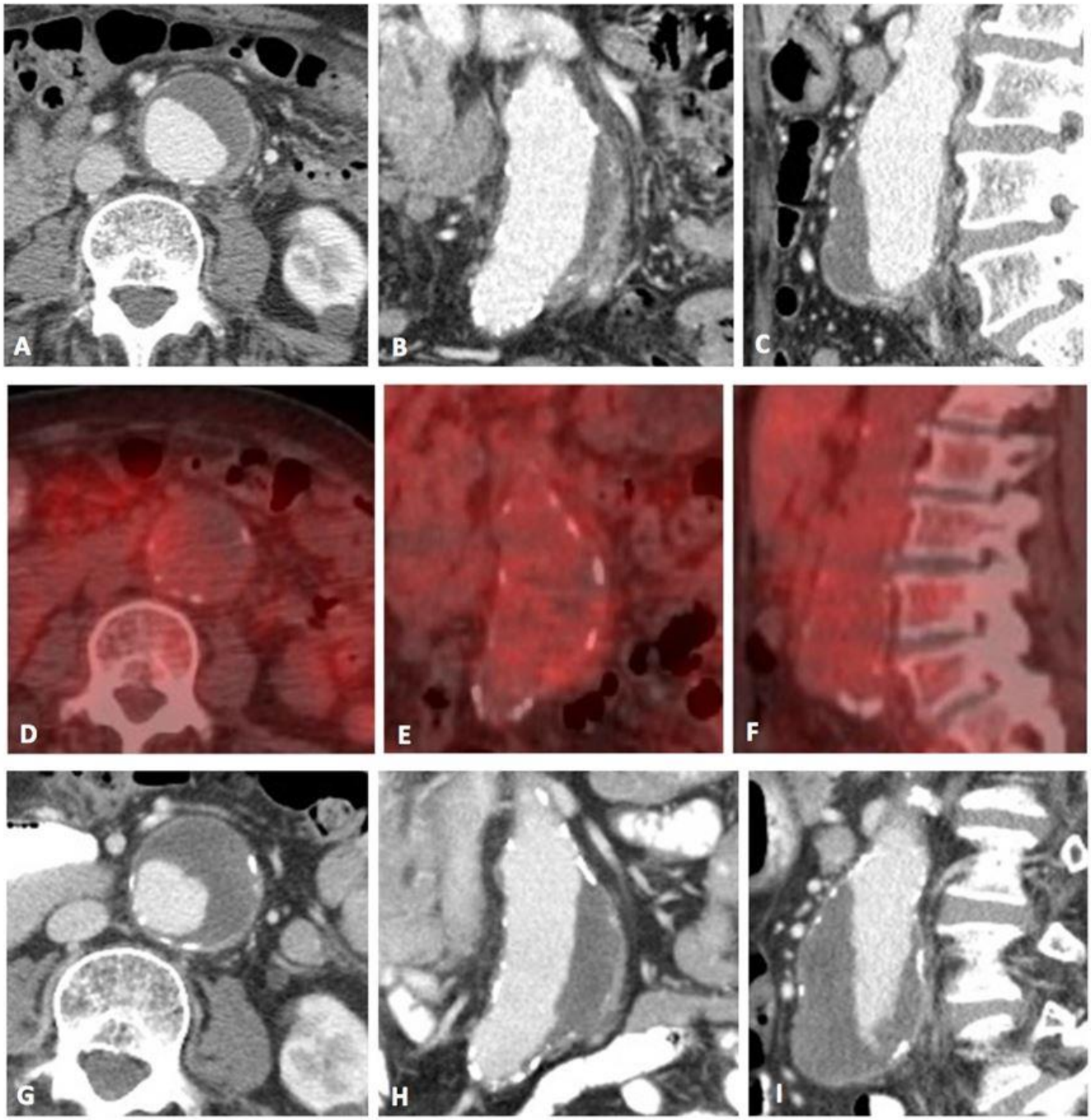


**Figure 10:** 88-year-old male with IgG4-related disease.

FINDINGS: Images are axial, coronal, and sagittal from left to right. A-C. A contrast-enhanced CT scan of the abdomen in the portal venous phase demonstrates an infrarenal aortic aneurysm (4.0 cm x 4.4 cm in largest trans-axial dimensions) with significant soft plaque. D-F. A concurrent fused PET-CT shows no appreciable FDG activity. G-I. Three months later, and 7 weeks into steroid treatment, a follow-up contrast-enhanced CT scan of the abdomen in the portal venous phase demonstrates stability of the aneurysm apart from increased non-calcified plaque.

TECHNIQUE: A-C. 64-slice CT, 200-230 mA, 120 kVp, 100 mL Omnipaque 350 IV contrast at 2.5 mL/sec, standard algorithm, axial 3.75 mm, coronal 2.5 mm, and sagittal 2.5 mm slice thickness. D-F. PET-CT, 18.6 mCi F18-FDG, 1 hour uptake period, multi-bed 3D acquisition, low mA CT attenuation correction (mA 30-65, kVp 140), axial 3.27 mm, coronal 5.47 mm, and sagittal 5.47 mm slice thickness. G-I. 64-slice CT, 210-250 mA, 120 kVp, 100 mL Omnipaque 350 IV contrast at 2.5 mL/sec, standard algorithm, axial 3.75 mm, coronal 3 mm, and sagittal 3 mm slice thickness.

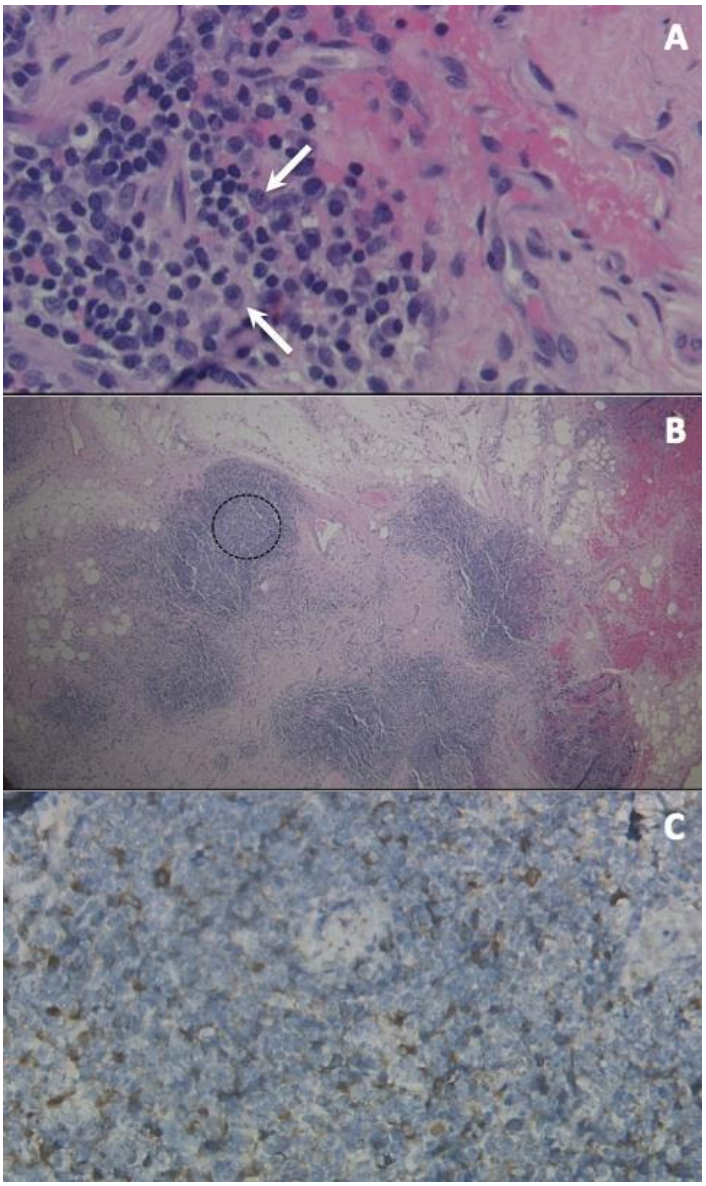


**Figure 11 (left):** 88-year-old male with IgG4-related disease. FINDINGS: Left lacrimal gland biopsy. A. Plasma cells (arrows) intermixed with other lymphocytes (H&E stain, magnification 600x). B. Lymphoid germinal centers (circle) on H&E stain at 20x. C. IgG4 immunostain (brown) using antibodies labeled with peroxidase (600x).





| | |
|---|---|
| **Etiology** | The etiology of IgG4-RD is poorly understood. IgG4 production appears to depend on T-helper 2 cell cytokines, which are involved in allergy and IgE production. An allergic reaction of the vasa vasorum may explain the presentation of periarteritis in IgG4-RD, with chronic inflammation contributing to remodeling and leading to aneurysms, pseudoaneurysms, and stenoses. |
| **Incidence and Prevalence** | Unknown but very rare. |
| **Gender Predilection** | Unknown. Based on 10 case reports, favors males 9:1. |
| **Age Predilection** | Unknown. Based on 10 case reports, mean age of 71.2 years. |
| **Risk Factors** | May be associated with allergic disorders (bronchial asthma, sinusitis, allergic rhinitis). |
| **Treatment** | Systemic steroid therapy is the mainstay of treatment. Immunosuppressants may be considered for refractory cases. In the treatment of coronary periarteritis with evidence of aneurysm or stenosis, surgical resection and bypass is favored over steroid therapy. Anticoagulants may be necessary with stenotic lesions. |
| **Prognosis** | Based on 10 case reports, coronary periarteritis successfully treated with steroids and/or surgical resection and bypass did not recur on short-term follow-up. The natural history and long-term follow-up of coronary periarteritis is not well studied. |
| **Imaging Findings** | On CT, appears as nodular or rind-like coronary arterial wall thickening. Stenosis, luminal ectasia, and aneurysm formation may be associated. Metabolic activity on PET imaging is variable. |

**Table 1:** Summary table for immunoglobulin G4-related coronary periarteritis.

| Differential | Clinical Presentation | CT Findings | PET Findings |
|---|---|---|---|
| **IgG4-Related Coronary Periarteritis** | Ranges from asymptomatic to symptoms of coronary ischemia or myocardial infarction. | Nodular or rind-like coronary arterial wall thickening. Stenosis, luminal ectasia, and aneurysm formation may be associated. | Variable FDG uptake. |
| **Kawasaki Disease** | Recent history of fever, conjunctival injection, mucositis, cervical lymphadenopathy, rash, and peripheral extremity edema or desquamation. | Coronary aneurysms, usually with calcifications and without pseudotumor formation. May stenose. | Unknown. |
| **Polyarteritis Nodosa** | Depends on organ involvement. Most common cardiac presentation is heart failure. | Coronary involvement may include stenosis, dilation, and dissection without pseudotumor formation. | Unknown. |
| **Takayasu Arteritis** | History of fever, fatigue, upper body pains, upper extremity pain and neuropathy. | Aortic and large vessel stenosis, dilation, and wall thickening. Coronary involvement rare but may include stenosis and aneurysms with possible calcifications. | Unknown. |
| **Churg-Strauss Syndrome** | History of allergic rhinitis, nasal polyposis, and bronchial asthma. Findings of myocarditis, heart failure, myocardial infarction, pericarditis, and pericardial effusion. | Coronary involvement rare but may include stenosis or giant aneurysms. | Unknown. |
| **Lymphoma** | "B symptoms" of fever, weight loss, night sweats, and generalized pruritis. Cardiac presentation includes pericardial effusion, heart failure, and AV block. | Enlarged or matted lymph nodes. May surround or encase coronary arteries. | Expected FDG uptake. |
| **Castleman's Disease** | Associated with HIV and HHV-8. May present with symptoms related to a mass in unicentric disease and "B symptoms" in multicentric disease. | Largely indistinguishable from lymphoma. Case report of a coronary pseudotumor with calcifications. | Unknown. |
| **Rosai-Dorfman Disease** | Bilateral painless cervical lymphadenopathy. | Homogeneous soft tissue densities and local lymphadenopathy. Masses may surround vessels, including coronaries, and are usually without significant calcifications. | Unknown. |

**Table 2:** Differential table of IgG4-related coronary periarteritis.

## ABBREVIATIONS

AV = atrioventricular
CT = computed tomography
CTA = CT angiography
ECG = electrocardiogram
FDG = 18F-2-fluoro-2-deoxyglucose
HHV-8 = human herpesvirus-8
HIV = human immunodeficiency virus
IgE = immunoglobulin E
IgG = immunoglobulin G
IgG4 = immunoglobulin G4
IgG4-RD = immunoglobulin G4-related disease
IVUS = intravascular ultrasound
MRI = magnetic resonance imaging
OCT = optical coherence tomography
PAN = polyarteritis nodosa
PET = positron emission tomography
SUV = standard uptake value

## KEYWORDS

immunoglobulin G4-related disease; coronary periarteritis; cardiac; computed tomography; PET

***Online access***
This publication is online available at:
www.radiologycases.com/index.php/radiologycases/article/view/1967

***Peer discussion***
Discuss this manuscript in our protected discussion forum at:
www.radiolopolis.com/forums/JRCR

***Interactivity***
This publication is available as an interactive article with scroll, window/level, magnify and more features.
Available online at www.RadiologyCases.com

Published by EduRad
www.EduRad.org